Research Square

Preprints are preliminary reports that have not undergone peer review.
They should not be considered conclusive, used to inform clinical practice,
or referenced by the media as validated information.

Rainfall Characteristics, Cloud Regimes and associated Microphysical Properties over the Lakshadweep Islands of India during the Summer Monsoon Season

Ambuj K Jha

ambuj.cat@tropmet.res.in

Indian Institute of Tropical Meteorology (IITM)

Harikrishna Devisetty

Indian Institute of Tropical Meteorology (IITM)

Kaustav Chakravarty

Indian Institute of Tropical Meteorology (IITM)

Rohit Patil

Indian Institute of Tropical Meteorology (IITM)

Research Article

Keywords: Lakshadweep, rainfall microphysics, Island region, summer monsoon rainfall

Posted Date: August 3rd, 2026

DOI: https://doi.org/10.21203/rs.3.rs-10151191/v1

License: This work is licensed under a Creative Commons Attribution 4.0 International License.
Read Full License

Additional Declarations: No competing interests reported.

Rainfall Characteristics, Cloud Regimes and associated Microphysical Properties over the Lakshadweep Islands of India during the Summer Monsoon Season

Ambuj K Jha[1,*], Harikrishna Devisetty[1], Kaustav Chakravarty[1], Rohit Patil[1]

[1]Atmospheric Research Test bed, Indian Institute of Tropical Meteorology (IITM), Ministry of Earth Sciences, India

*Correspondence to: ambuj.cat@tropmet.res.in

ABSTRACT Rainfall and cloud properties along with microphysical characteristics are less known over the island regions of India. The present study examines the spatial distribution of climatological rainfall characteristics, rainfall amount (RA), rainfall frequency (RF), and rainfall rate (RR), along with the vertical structure of precipitation. We use 16 years (1998–2013) of TRMM precipitation radar data at ~5 km × 5 km resolution during the summer monsoon season (June–September) over the Lakshadweep region. In addition, rainfall microphysical features are examined using disdrometer data collected at Agatti Island during the 2024 summer monsoon. Climatological RA ranges from 6-12 mm/day across the islands and is relatively higher over the eastern islands. RF follows similar pattern while RR shows contrasting distribution of localized pockets of high values. While total rainfall is contributed by both RF and RR, RF plays dominant role. Frequency distribution of echo top heights (ETH) shows bimodal nature (4 km and 6 km); more than 60% of the precipitating clouds have ETH between 5-8 km. Though TRMM broadly provides convective-stratiform classification, we reclassify the precipitating clouds into 4 categories, deep convective, pure stratiform, mixed and shallow convective. Our analysis reveals that Lakshadweep region is strongly dominated by stratiform-like precipitation, associated with mixed and stratiform clouds, accounting for 75% occurrences and nearly 70 % of the total rainfall. The remaining precipitation is associated with shallow and deep convective clouds, which account for 20% and 5% occurrences and contribute about 16 % and 15 % of the total rainfall, respectively. Rainfall microphysical features show bimodal distributions of mass-weighted drop diameter (Dm) and generalized intercept parameter (Nw). Modes for Dm occur at 1-1.2 mm and 1.6 mm while those for log10(Nw) occur at 3.2 and 3.8. Diurnal variations of RR and Dm are weak and show complex pattern with multiple peaks, primarily during nocturnal and late evening hours. Background atmospheric conditions show dry air intrusion at mid-tropospheric levels in the

offshore Arabian sea along with high CAPE and CIN values compared to the coastal region, which influence cloud development in this region.

Keywords: Lakshadweep, rainfall microphysics, Island region, summer monsoon rainfall

1. Introduction

The Indian summer monsoon (ISM), one of the most prominent world's monsoon systems, is often referred to as the "lifeline of India". ISM has a profound impact on agriculture, water resources and socio-economic well-being of more than 1.5 billion people who inhabit the subcontinent. It is characterized by the seasonal reversal of winds and copious rainfall from June to September. On an average, ISM contributes nearly 80 % of India's total annual rainfall (Ananthakrishnan et al. 1983). Influenced by both internal dynamics and external forcings, ISM exhibits a large spatial and temporal variability in rainfall over the country (e.g., Rao 1976; Dhar et al., 1978; Parthasarathy and Mooley 1978; Krishnamurthy and Shukla 2000). Several past studies elucidated the large-scale characteristics of precipitation and its types over the Indian region and adjoining seas using satellite data (Houze et al. 2007; Romatschke and Houze 2011; Saikranthi et al. 2014; Bhat and Kumar 2015). These studies showed that ISM rainfall is heavily concentrated over 3 regions, the Himalayan foothills, the Western Ghats and the Myanmar coast. They further reported that stratiform precipitation dominates over most parts of the region, except over the Western Ghats, where convective rainfall is more prevalent. Overall, 46% rainfall is stratiform, 44% is convective and remaining 10 % is categorized as others (Romatschke and Houze 2011). Rainfall also exhibits spatio-temporal heterogeneity in microphysics and associated rain drop size distribution (DSD) (Rao et al. 2009; Radhakrishna et al. 2009; Chakravarty et al. 2013; Konwar et al. 2014; Jha et al. 2022; Rakshit et al. 2024). DSD is closely linked to cloud microphysical and dynamical processes (Heymsfield et al. 2010) and important not just for understanding precipitation processes in a cloud (Rosenfeld and Ulbrich 2003) but also for improving quantitative estimates of rainfall using weather radars (Marshall et al. 1947; Bringi et al. 2003). DSD variation is complex, involves several microphysical processes such as collision-coalescence, break-up, evaporation and size sorting and occur even within a rain spell (Tokay and Short 1996; Rosenfeld and Ulbrich 2003; Atlas and Ulbrich 2006).

Over the Indian region, most of the available scientific literature on rainfall and associated DSD features is centered on the mainland locations of India, with relatively sparse coverage of the island territories and other peripheral regions. Some of the reasons are better logistical accessibility, observational infrastructure, higher population density and long-term data availability in mainland areas. In the past, a few studies have analysed the variability and long-term trends of rainfall over Lakshadweep islands (Sreekesh 2016; Sridhar and Pai 2023). More recently, Rakshit et al. (2024) studied the rain DSD characteristics over Kavaratti Island using impact disdrometer data and found a predominance of larger drops associated with high convective available potential energy (CAPE) values. However, these studies focused on local features based on point measurements and spatial characteristics of rainfall and associated nature of clouds remain largely unexplored.

Lakshadweep, an archipelago of 36 islands, is situated ~200-400 km off the west coast of India in the southeast Arabian sea (Fig. 1). The islands have coral reefs and a total area of 32 sq. km. In the context of ISM, Lakshadweep has unique geoegraphical and meteorological importance. It is in the direct path of the ISM low level jet and therefore, provides early indication of monsoon evolution and onset. Rainfall is predominantly maritime in nature and ideal for studying oceanic monsoon systems and processes. The present study defines Lakshadweep region (LR) as the region extending from 8-12°N and 72-74°E which includes all islands and the surrounding sea (Fig.1a,b). Geographically, most islands in the LR are clustered within a small region, except for Minicoy, which is located far south and separated from the main cluster. The precipitation radar (PR) onboard Tropical Rainfall Measuring Mission (TRMM) satellite provides high-resolution 3D vertical structure of precipitation (Kummerow et al., 1998, 2000; Kozu et al. 2001). We utilize TRMM PR data to examine the climatological characteristics of rainfall and precipitating clouds over the LR. The microphysical features of rainfall are studied using the data collected with an impact disdrometer installed at Agatti island.

Specifically, we address following questions over LR

1. What is the spatial distribution of rainfall features, viz., rainfall amount, rain rate and frequency across the LR?
2. What is the dominant mode of precipitating clouds?
3. What are the characteristics of rainfall DSD and what rainfall microphysical processes govern rainfall formation in this region?

4. What thermodynamic and dynamic conditions are prevalent over this region?

The remainder of the paper is organized as follows. Section 2 describes the data and methodology, section 3 shows results, section 4 contains discussions followed by conclusions in section 5.

2. Data and Methodology

2.1. Disdrometer

The Indian Institute of Tropical Meteorology (IITM) Pune has installed an impact-type Joss-Waldvogel disdrometer (JWD, Joss and Waldvogel, 1967) model RD-80 at Agatti island in Lakshadweep in the year 2024. Data corresponding to ISM 2024 (June-September) has been analysed in this study. The JWD measures rainfall DSD by converting the mechanical momentum of falling rain drops into electrical pulse. The amplitude of this pulse is proportional to the size of the rain drop. The JWD has an effective sampling area of 50 cm^2 and measures drop sizes with an accuracy of ±5% provided the drops are evenly distributed over the sensor surface. It classifies raindrops into 127 discrete size classes. However, the standard output consists of 20 non-uniform size bins ranging from 0.3 to 5.4 mm (Distromet, 2002). The bin widths increase with drop diameter, varying from 0.1 mm to 0.5 mm. JWD, while widely considered a reliable instrument for DSD measurements (Tokay et al. 2001), has some limitations. It underestimates the number of smaller drops in heavy rain because of the "dead time" of the sensor (Tokay and Short 1996). To correct this, the manufacturer provides a correction matrix that compensates for the loss of smaller drop counts (Sheppard and Joe 1994). The detection of smaller drops is also suppressed by background noise (Tokay et al. 2003). The instrument is also limited in measuring very large drops of diameter>5 mm. Additionally, the assumption of terminal fall velocity in JWD can also result in erroneous DSD under the influence of vertical air motion (updrafts or downdrafts) (Salles and Creutin 2003; Tokay et al. 2003). Despite these shortcomings, JWD remains widely used for rainfall microphysical studies and DSD parameterization (Tokay and Short 1996).

The JWD provides DSD spectra every 30 s. To account for the noise and sampling limitations, we considered a DSD sample valid only if it contains at least 10 drops and corresponds to a rain rate

125 greater than 0.1 mm h^{-1} (Tokay et al. 2001). Samples not meeting these criteria are treated as noise
126 and excluded from further analysis.

127 For each valid sample, we computed rain rate (RR), mass weighted mean drop diameter (Dm),
128 liquid water content (LWC), reflectivity (Zjwd) and generalized intercept parameter (Nw) using
129 the equations given below (Tokay and Short 1996).
130
131 RR (mm/h) is given by

132 $$RR = \frac{6\pi}{10^3}\frac{1}{A \times t}\sum_{i=1}^{20}(n_i D_i^3) \quad (1)$$

133 where A (m^2) is the sampling area of the JWD, t (seconds) is the sampling interval, n_i the drop
134 count in size class i, and D_i (mm) the mean drop diameter.
135 The drop number concentration N(Di) (m^{-3} mm^{-1}) corresponding to size class i is calculated as,

136 $$N(D_i) = \frac{n_i}{A.t.V(D_i).\Delta D_i} \quad (2)$$

137 where, $V(D_i)$ (m s^{-1}) is the (theoretical) terminal velocity (Gunn and Kinzer, 1949) and ΔD_i (mm)
138 is the diameter interval of size class i.
139 The nth moment of the DSD is given by,

140 $$M_n = \sum_{i=1}^{20} N(D_i) D_i^n \Delta D_i\,, \quad (3)$$

141 Dm (mm) is calculated as (Bringi and Chandrasekar, 2001)

142 $$Dm = \frac{M_4}{M_3} \quad (4)$$

143 Zjwd calculated from JWD data, Zjwd (mm^6 m^{-3}) is given by

144 $$Zjwd = \sum_{i=1}^{20} N(D_i) D_i^6 \Delta D_i \quad (5)$$

145 Zjwd is converted to dBZ units using the expression 10 $\log_{10}$(Zjwd).
146 LWC is calculated using the formula below

147 $$LWC = \frac{\pi}{6000}.\rho_w.\sum_{i=1}^{20} D_i^3 \frac{n_i}{A.t.V(D_i)} \quad (6)$$

148 Nw (m^{-3} mm^{-1}) represents the number concentration of rain drops and is calculated from Dm and
149 LWC (Bringi et al., 2003) as below

$$Nw = \frac{4^4}{\rho_w} \frac{10^3 LWC}{Dm^4} \quad (7)$$

2.2. TRMM

TRMM, a joint venture between National Aeronautics and Space Administration (NASA) and Japanese Aerospace Exploration Agency (JAXA) was launched in November 1997 (Kummerow et al., 1998). The PR onboard TRMM was the first spaceborne weather radar designed to provide 3D vertical structure of precipitation in the tropics and subtropics in the latitude band from ~36°S-36°N (Kummerow et al., 1998, 2000; Kozu et al. 2001). PR operates at a frequency of 13.8 GHz (Ku-band) and scans in the cross-track direction at an inclination of 17° with a swath width of 215 km (245 km after the orbital boost). The horizontal footprint size is ~4-6 km and vertical resolution is 250 m at nadir. There are 80 vertical levels from the surface to 20 km; lowest level is defined as the Earth ellipsoid and heights are measured relative to the Earth ellipsoid. The minimum detectable signal of TRMM PR is approximately 18 dBZ (e.g., NASDA 1999), corresponding to the rain rate of about 0.4 mm/h (Schumacher and Houze 2003).

2.2.1. Rainfall climatology

In this study, we have used TRMM PR products for a 16-year period (1998-2013) to obtain the summer monsoon climatology over the LR. All PR data are from version 7. TRMM PR product 2A25 (Iguchi et al. 2000) provides "near-surface" rain rates from the range bin closest to the surface generally not affected by the clutter. The near-surface rain rates are used to obtain the mean rain rate (RR, mm/h), rain frequency (RF, %) and mean rain amount (RA, mm/day) for the 16-year period. RR is obtained by summing all the samples of rain rates>0 and dividing it by total number of PR overpasses (N) over a grid. RF is calculated by dividing number of raining pixels by N while RA is estimated by averaging all raining samples and producing a daily equivalent value. For processing of PR products, data collected from each individual swath is binned onto a 0.05 resolution regular grid (~5 km×5 km) and then averaged over the study period to produce the high-resolution mean climatology.

2.2.2. Types of precipitating clouds

Tropical precipitation is mainly classified into two types: convective and stratiform (Houze 1993). However, the separation is not always unambiguous and there exists a "mixed" rain formed from a decaying convective cell in transition to stratiform rain (Williams et al., 1995). The microphysical properties of the mixed rain are intermediate to pure convective and stratiform types and therefore, can be considered a separate rain class. These three rain types are associated with deep clouds extending above the melting layer and contain frozen hydrometeors. Additionally, rain in tropics also forms from shallow clouds which are confined below the melting level and do not involve ice-phase processes (Williams et al., 1995).

TRMM identifies three types of precipitation, convective, stratiform and other; category "other" mostly contains noise and anvil clouds (Awaka et al., 2009). The classification is based on vertical profiles of reflectivity (hereafter, referred as Z) and the horizontal variability of the echo. Based on how strongly a data point satisfies the classification criteria, the TRMM algorithm assigns a confidence level to that data point specified by "rainType" value. For example, rainType 100 has high confidence for stratiform rain while rainType 200 includes pixels with pure convective rain. TRMM also designates pixels as "shallow rain" if the top height of the echo is 1.5 km below the climatological 0°C. Thus, classification of clouds is not trivial and associated with uncertainties.

In this study, we reclassify the precipitating clouds into 4 categories over the study region, namely deep convective, pure stratiform, mixed and shallow convective based on the vertical profiles of Z and rainType values. A precipitating cloud is identified if Z $\geq$30 dBZ at two consecutive range bins below melting layer. The precipitating clouds are then classified as follows: (1) shallow convective clouds, if the echo-top height is below the freezing level height; (2) deep convective clouds, if rainType = 200; (3) pure stratiform clouds, if rainType = 100; and (4) mixed clouds, comprising the remaining precipitating clouds that do not satisfy the above criteria. During the classification, it was ensured that no overlapping occurs among the four cloud categories. For brevity, the precipitating clouds are called clouds/rain and the four categories are called shallow, deep, mixed and stratiform.

A contoured frequency by altitude diagram (CFAD, Yuter and Houze 1995) of radar reflectivity is constructed using all profiles of Z extracted over LR. CFADs have been constructed with 2 dBZ

reflectivity bins at 0.25 km height interval between 0.5 and 20 km. At each altitude level, the frequency of occurrence is normalized by the maximum frequency across all levels and a grid is considered only if the normalized frequency is at least 10% (Jha et al. 2022).

2.3. Other data

Background atmospheric conditions are examined from the monthly European Centre for Medium-Range Weather Forecasts (ECMWF) Reanalysis v5 (ERA5) dataset available at a grid resolution of 0.25° x 0.25° (Hersbach et al. 2020). To assess the atmospheric instability, CAPE is used. CAPE is widely considered a measure of strength of atmospheric convection and presents the amount of energy released by an air parcel when it is lifted pseudo-adiabatically from the level of free convection (LFC) to level of neutral buoyancy (Mapes and Houze 1992).

3. Results and Discussions

3.1. Rainfall features

Figure 2 shows the spatial distributions of RA (mm/day), RF (%) and RR (mm/h). RA increases from the Arabian sea towards the coast, peaks over the terrain of the Western Ghats and then drastically decreases on the lee side of the Ghats (Fig. 2a). The increase in rainfall towards coastal region is due to the blocking effect of the WG mountains which exerts a strong control on low-level moist air flow and distribution of ISM rainfall in this region (Grossman and Durran 1984; Xie et al. 2006; Romatschke and Houze 2011; Flynn et al. 2017). However, offshore rainfall over the Arabian sea is mainly controlled by the sea surface temperature and not by the WG (Sijikumar and Rajiv 2012; Zhang and Smith 2018). Over Lakshadweep islands, a slight west-east gradient can be seen and eastern islands such as Andrott and Kalpeni receive higher RA. Within the island cluster, RA values do not differ much and range from 6-12 mm/day with highest over Kiltan (12 mm/day) and lowest over Kavaratti (5 mm/day).

RF also shows similar pattern with progressive higher values towards the coast, maximum over the WG and then decreases to the east (Fig. 2b). However, RF has a wider zone of higher values than RA. Here too, the values are nearly similar among the islands and eastern islands have higher RF. In contrast to RA and RF, the spatial pattern of RR is different and does not show a systematic

increase towards the coast; instead, localized pockets of high RR (~9-10 mm/h) are scattered over the offshore region, indicating occurrence of high RR events. Note that over LR, both RF and RR contribute to RA but RF plays dominant role, similar to that observed over the Western Ghats mountains (Shrestha et al. 2015; Ambuj et al. 2025).

3.2. Nature of clouds

A key question that arises: what is the nature of precipitating clouds over the LR. Echo top height (ETH) is commonly taken as a proxy for vertical development of clouds by considering a threshold value of Z,i.e., higher the ETH, deeper is the cloud. The ETH for TRMM corresponds to its sensitivity of 17 dBZ. Fig. 3a shows mean ETH above surface level. Deeper storms are prevalent over the open sea while shallower storms occur over the WG terrain, consistent with previous studies (Shrestha et al 2015; Utsav et al. 2017; Ambuj et al. 2025). Over the LR, mean ETH are typically between ~6-7 km which are associated with moderate RR events and modulate the rainfall features over the region. The frequency distribution of storm top heights along with cumulative distribution is shown in Fig. 3b. A bimodal distribution is evident with a primary mode around 6 km and the secondary mode near 4 km. The secondary mode corresponds to shallow precipitating clouds with ETH below the melting layer while the primary mode is associated with moderately deep clouds. The distribution also shows a long tail associated with very deep convection. More than 60 % of the precipitating clouds have ETH between 5-8 km while clouds with ETH> 10 km occur <2% of the time (Fig. 3b). These results suggest that moderately deep clouds dominate the cloud population over the study region while very deep clouds occur only sporadically.

A related question concerns the dominant type of precipitating cloud over this region. Fig. 4 shows the occurrence frequency of all 4 categories of clouds and their respective rain fractions. Mixed and stratiform clouds clearly dominate the cloud population over the LR and surrounding region. Both exhibit comparable occurrence frequencies of about 40–50% across much of the LR, followed by shallow clouds (~15–25%). Convective clouds are the least common, with occurrence frequencies generally below 10% (Fig. 4a–d). The rainfall fraction broadly follows a similar pattern (Fig. 4e-h). Mixed clouds are the largest contributors to total rainfall, accounting for nearly 50% of the accumulated rainfall over the region. Stratiform clouds contribute only about 20–30%

of the total rainfall even though they occur as frequently as mixed clouds. Shallow clouds have a rain fraction of about 15–20%, while convective clouds contribute the least overall rainfall. Note that the spatial distribution of convective clouds is characterized by a scattered and speckled pattern with small isolated pixels of higher values (Fig. 4a,e). In contrast, other clouds exhibit a more spatially coherent distribution. This pattern is likely associated with localized, short-lived convective cells embedded within large MCS or occurring as isolated convective clouds (Houze, 1997).

The cumulative occurrence frequencies of convective, stratiform, mixed, and shallow clouds over LR are 5%, 38%, 37%, and 20%, respectively (Fig. 5a). The respective rainfall fractions are 14%, 22%, 48%, and 16%. Note that even though stratiform and mixed rain have comparable occurrence frequencies, mixed clouds contribute more than twice the rainfall produced by stratiform clouds. Overall, the results demonstrate the dominance of mixed and stratiform precipitation over the Lakshadweep region. The large contribution of mixed clouds to both total occurrence and rainfall highlight the importance of classifying them as a separate precipitation category rather than grouping them with conventional convective or stratiform classes.

To examine the vertical structure of precipitation, CFAD of Z is constructed and shown in Fig. 5b. The total number of Z profiles considered is 1328005. Similar to Fig. 3b, CFAD shows a bimodal structure, one above and the other below the melting layer. A distinct melting layer signature is seen ~4 km altitude, indicative of stratiform dominated precipitation regime. High Z values (>40 dBZ) have low frequency of occurrence and the vertical extent of CFAD is up to 9 km. This suggests that deep, intense convective cores are not common over LR and moderate rainfall is prevalent over this region, as discussed earlier. The primary mode of CFAD occurs around 30 dBZ at the lower levels between 1-3 km. A secondary mode is seen at higher level between 5-6 km and shows lesser Z values of 19-21 dBZ associated mainly with ice particles.

3.3. Agatti rainfall

TRMM PR provides vertical profiles of rain rate. Fig. 6 shows the cross-section of rain rate profiles along the latitude of Agatti (10.8°N). The vertical structure of RR also shows typical characteristics of stratiform rain, with higher RR near the surface (>6 mm/h) and a sharp gradient around the melting layer (above 4.5 km), where RR drops to 1 mm/h. Over the offshore locations, RR profiles

exhibit higher values and decrease towards the inland regions. RR profiles show particularly high values between 71.5-72°E, indicative of deep convective rain events in this region. Over Agatti, RR profile has moderate values and stratiform rain processes appear dominant.

3.3.1. Rainfall Microphysics

To understand the rainfall microphysical processes at Agatti Island, we investigate rainfall parameters calculated using JWD data (Fig. 7). The distribution of Dm is bimodal in nature with a primary mode between 1-1.2 mm and a minor secondary peak at 1.6 mm (Fig. 7a). Different modes suggest association with different types of clouds and different microphysical processes. The primary mode with small to mid-sized drops is likely associated with stratiform and shallow clouds whereas the secondary mode is likely contributed by mixed clouds and deep clouds. Precipitation in stratiform clouds typically forms in weak updrafts (<1 m/s) from ice crystals which aggregate to large snowflakes and melt to rain drops during fall (Rosenfeld and Ulbrich, 2003). In shallow clouds, drops primarily grow through collision-coalescence but do not have sufficient time to grow to larger sizes. In contrast, mixed and deep clouds have stronger updrafts which allow hydrometeors to remain suspended for a long time and grow bigger through collision-coalescence and accretion of cloud droplets, both on water and ice hydrometeors (Rosenfeld and Ulbrich, 2003).

Z shows a unimodal distribution and a broad mode occurs between 20-25 dBZ (Fig. 7b). The distribution is broader and values range from 5-50 dBZ. High Z values (>40 dBZ) occur only 5% of the time and likely associated with mixed or deep convective clouds. In case of LWC, major fraction (~90%) of values are within 0.4 g/m^3 and a longer tail is also seen in the distribution (Fig. 7c). The distribution of log10(Nw) has a bimodal pattern similar to Dm; modes occur around 3.2 and 3.8. Nw skews towards higher concentration of rain drops. Note that Nw has inverse relationship with Dm. Higher Dm values correspond to lower Nw and vice versa.

Now, we examine the DSD spectrum (Fig. 8) over Agatti. A primary peak is seen at 0.5 mm and a minor peak at 1.1 mm. The curve shows a monotonic decrease in the number concentration of drops bigger than 1.1 mm. Thus, the DSD spectrum over Agatti is predominantly characterized by "maritime-like" regime which exhibits larger concentration of small to mid-sized drops.

3.3.2. Diurnal variation

Fig 9 shows the diurnal variation of RR and Dm. RR shows multiple diurnal peaks, one minor peak in the nocturnal hour (0300 LT) and two prominent peaks in the morning (1000 LT) and the late afternoon to evening hours (1800-2000 LT). In a recent study, Rakshit et al. (2024) analysed diurnal cycle of RR using JWD data over Kavaratti island in the LR. A similar diurnal behaviour was seen with diurnal peaks at nocturnal, morning and late afternoon hours; however, the amplitudes of all peaks were comparable. Flynn et al. (2017) also observed a noisy diurnal cycle of RR in the "well offshore region" of the Arabian sea (similar to LR here) with multiple diurnal peaks, primarily in the morning and late afternoon hours. They attributed this variability to high instability conditions, indicated by high CAPE values preceding rainfall maxima in offshore regions.

Dm also shows a complex diurnal pattern; minor peaks in the nocturnal hours and prominent peaks during morning to late afternoon hours (0800-2000 LT). Rakshit et al. (2024) also showed similar diurnal behaviour of Dm with multiple peaks. Here, Dm values are relatively lower in the nocturnal hours and increase during morning to late afternoon hours. While Dm and mean RR show some diurnal variation, DSD suggests that diurnal variation is not prominent (Fig. 9c). Small to mid-size drops (< 2 mm) show persistent dominance throughout the day. Bigger drops >4 mm also prevail throughout the day, but concentration is lower. DSD broadening, though minor, is seen during morning hours (0800-1000 LT) and nocturnal hours. There are only subtle variations in the spread towards larger sizes. Thus, DSD appears stable and less sensitive to the diurnal forcing.

3.4. Atmospheric conditions

In this section, we examine the background atmospheric conditions over LR and the surrounding region. Fig. 10a shows the longitude-pressure cross section of RH across Agatti, overlaid with temperature contours. A warm and moist marine boundary layer can be seen where RH is around ~80-100 %. At the mid-tropospheric levels (between 450-650 hPa), an intrusion of dry layer of air (RH~50-60%) is observed from the western Arabian sea, extending to nearly 74°E. The thickness of this layer decreases towards the east and the atmosphere becomes increasingly moist through much of the lower and middle troposphere. Past aircraft campaigns such as CAIPEEX

(Maheskumar et al. 2014) and INCOMPASS (Fletcher et al. 2020) have reported similar incursion of dry air from the Arabian deserts into mid-tropospheric levels which tends to suppress convection in the Arabian sea. Fletcher et al. (2020) suggested that these dry air intrusions allow build-up of humidity in the boundary layer and may result in high CAPE values. However, unlike land, CAPE is often weakly related or anti-correlated with rainfall over tropical oceans (Thompson et al. 1979; Mapes and Houze, 1992; Lin and Johnson, 1996; Fletcher et al. 2020).

Here, CAPE shows higher values in the offshore region and decreases towards the coast and the orographic region of the Western Ghats (Fig. 9b). Within LR, CAPE is around 850-1000 J/kg with the highest values for the southernmost island, Minicoy. However, high CAPE does not necessarily lead to convection occurrence because the air parcel needs to overcome the negative energy barrier between the surface and the LFC. This energy barrier is called CIN and suppresses convection even though CAPE is high. Here, CIN is also moderately higher in the offshore region (Fig. 9c) and shows values of 60-90 J/kg. Both CAPE and CIN decrease from west to east. Previous studies using radiosonde data collected over Arabian sea have reported that the vertical thermal structure is complex over Arabian sea and frequent inversions occur in the lower and middle tropospheric layers (Bhat 2005; Maheskumar et al. 2014; Fletcher et al. 2020). These multi-level inversions have been found to be associated with the advection of warm and dry air from surrounding desert regions and its subsidence (Johnson et al. 1996; Bhat 2005; Maheskumar et al. 2014). This can elevate CIN by increasing static stability and suppress the formation of deep convection and favor moderate or shallow cloud tops.

Further, we also examine the vertical section of equivalent potential temperature (θe) across Agatti (Fig.11). The vertical gradient of θe is a primary indicator of convective instability and is analogous to moist static energy. θe shows high values (>350 K) within the boundary layer and decreases to minimum (~330 K) in the mid tropospheric levels between 600-700 hPa, associated with incursion of dry air. Note that the vertical gradient becomes weaker as we move eastward towards the coast. Additionally, the low-level winds also show a slight reduction in strength from offshore to coastal regions with a shear at low and middle tropospheric levels. In summary, these results indicate relatively higher convective instability over the offshore Arabian sea, accompanied by a complex thermodynamic structure that influence the vertical growth of convection.

4. Discussion

The Lakshadweep islands exhibit weak spatial variability in rainfall characteristics. RA and RF show only minor differences among the islands, while the variability in RR is even smaller. This suggests that the precipitation regime over the LR is broadly uniform. Nearly 70% of the total rainfall comes from mixed precipitating clouds, which form from decaying convection transitioning into stratiform clouds. Houze (1997) noted that the transition/intermediary region is more similar to the stratiform region in terms of microphysical and dynamical processes, and therefore, considered mixed rainfall under the broader spectrum of stratiform regime. Thus, statistically, LR is strongly dominated by stratiform-like precipitation (mixed and stratiform clouds) and accounts for 75 % occurrences and nearly 70% of the total rainfall. The convective precipitation regime includes the remaining two cloud types, shallow and deep convective. Interestingly, shallow clouds dominate the population of this regime and contribute 16 % of the total rain, slightly higher than deep convective clouds (14%). Higher occurrence of shallow clouds could be associated with dry-air incursion that suppress the formation of deep clouds.

An important question that arises is why stratiform precipitation is dominant over LR? Schumacher and Houze (2003) studied convective-stratiform statistics in the tropics using TRMM PR data and found that oceans, in general, have a larger fraction of stratiform rain compared to land. They attributed this to the near-moist adiabatic stratification of the free atmosphere. The updrafts over the oceans are moderate at all the levels and favor weaker but longer-lived convection capable of generating and maintaining large stratiform regions. In addition, a warm and moisture-rich marine boundary layer with weak diurnal variation helps to sustain the convection. Thus, there is continuous formation of convective cells which can extend to greater heights and subsequently lead to effective production of stratiform rain.

The diurnal variation of DSD over Agatti (Fig. 9c) is weak and noisy, suggesting limited diurnal modulation of convection in this region. The thermodynamic and dynamic conditions are complex and characterized by incursion of dry air at mid-tropospheric levels, high CAPE, high CIN, multiple inversion layers along with wind shear. These suggest high convective potential but also some inhibition and may favor the development of episodic vigorous convection. However, the

mechanisms governing the formation, evolution, and maintenance of different cloud types over the marine environment of LR are not clear and require further investigation. More in-situ measurements along with ground-based radar observations in the future could provide valuable insights into the structure, evolution, and organization of precipitation systems over this region.

5.Conclusions

The study utilizes 16 years (1998–2013) of TRMM PR V7 data at 0.05° × 0.05° resolution during the summer monsoon season (June–September) to characterize the spatial distribution of rainfall and the vertical structure of precipitating clouds over the Lakshadweep region. Rainfall characteristics [rainfall amount (RA), rainfall frequency (RF) and rainfall rate (RR)] along with type of rainfall are examined. In addition, rainfall microphysical properties are analysed using disdrometer data collected during ISM 2024 at Agatti island. Though TRMM broadly provides convective-stratiform classification, we reclassify the precipitating clouds into 4 categories, deep convective, pure stratiform, mixed and shallow convective. The major findings of this study are summarized as below:

1. Climatological RA over the Lakshadweep region ranges from 6-12 mm/day and is relatively higher for eastern islands (Kalpeni, Andrott and Kiltan); RF shows similar pattern as RA but RR displays a distinct pattern of localized high values.
2. Total rainfall is contributed by both RF and RR but the former plays the dominant role.
3. Frequency distribution of echo top heights (ETH) is bimodal, with peaks at ~4 km and ~6 km. More than 60% of the precipitating clouds have ETH between 5-8 km, indicating that moderate cloud tops dominate this region.
4. Lakshadweep region is strongly dominated by stratiform-like precipitation, associated with mixed and stratiform clouds, accounting for 75% occurrences and nearly 70 % of the total rainfall. In comparison, shallow and deep convective clouds account for 20% and 5% occurrences and contribute about 16 % and 14 % of the total rainfall, respectively.
5. Rainfall microphysics reveals bimodal structure of Dm and Nw with primary mode for Dm [log10(Nw)] at ~1-1.2 mm (~3.2) and secondary mode at ~1.6 mm (~3.8).
6. Diurnal variations of RR and Dm are weak and show multiple peaks, primarily in the morning and afternoon hours.

7. The offshore Arabian Sea is characterized by a mid-tropospheric dry-air intrusion along with elevated CAPE and CIN relative to the coastal region, indicating enhanced convective potential accompanied by moderate inhibition.

Acknowledgments

IITM is an autonomous organization and fully funded by the Ministry of Earth Science, Govt. of India. Authors are thankful to the Director, IITM, for the wholehearted support and encouragement in this work. Authors acknowledge Dr G Pandithurai (former Project Director, ART) and Dr B Padma Kumari (Project Director, ART) for the kind guidance, resources and valuable support. The sincere efforts of CMLRE staff involved in observations and maintenance at the disdrometer site are thankfully acknowledged.

Data availability Statement

The data that support the findings of this study are available from the corresponding author upon reasonable request.

Funding

The authors declare that no funds, grants, or other support were received during the preparation of this manuscript.

Competing Interests

The authors declare that they have no financial or non-financial interests that are directly or indirectly related to the work submitted for publication.

References

Ambuj, J.K., Bhat, G.S., Kalapureddy, M.C.R., Pandithurai, G., 2025. Radar-derived rainfall distribution over the Western Ghats of India: Investigating orography–dynamics interactions. Mon. Wea. Rev. 153, 1301–1313. https://doi.org/10.1175/MWR-D-24-0144.1.

Ambuj, J.K., Bhat, G.S., Kalapureddy, M.C.R., Pandithurai, G., 2022. Characteristics of rain events of different durations at a high-altitude site in the Western Ghats of India. Meteorol. Atmos. Phys. 134, 1–14. https://doi.org/10.1007/s00703-022-00902-9.

Ananthakrishnan, R., Pathan, J. M., & Aralikatti, S. S. (1983). The onset phase of the southwest monsoon. Current Science, 52, 155–164.

Atlas, D., and C. W. Ulbrich, 2006: Drop size spectra and integral remote sensing parameters in the transition from convective to stratiform rain. Geophys. Res. Lett., 33 .L16803, doi:10.1029/2006GL026824.

Awaka, J., Iguchi T. , Kumagai H. , and Okamoto K. , 1997: Rain type classification algorithm for TRMM precipitation radar. IGARSS'97: Remote Sensing; A Scientific Vision for Sustainable Development, T. I. Stein, Ed., Vol. 4, IEEE, 1633–1635, doi:10.1109/IGARSS.1997.608993.

Bhat, G. S. (2005), Convection inhibition energy of the inversion and the suppressed rainfall over the Arabian Sea during July 2002, Mausam, 56, 89–96.

Bhat, G. S., and S. Kumar, 2015: Vertical structure of cumulonimbus towers and intense convective clouds over the South Asian region during the summer monsoon season. J. Geophys. Res. Atmos., 120, 1710–1722, doi:10.1002/2014JD022552.

Bringi, V.N., Chandrasekar, V., 2001. Polarimetric Doppler Weather Radar: Principles and Applications. Cambridge Univ. Press, Cambridge, UK.

Bringi, V.N., Chandrasekar, V., Hubbert, J., Gorgucci, E., Randeu, W.L., Schoenhuber, M., 2003. Raindrop size distribution in different climatic regimes from disdrometer and dual-polarized radar analysis. J. Atmos. Sci. 60, 354–365. https://doi.org/10.1175/1520-0469(2003)060<0354:RSDIDC>2.0.CO;2.

Chakravarty K, Raj PE, Bhattacharya A, Maitra A (2013) Microphysical characteristics of clouds and precipitation during pre-monsoonand monsoon period over a tropical Indian station. J. Atmos. Sol.-Terr. Phys. 94: 28–33. https://doi.org/10.1016/j.jastp.2012.12.016.

Das, S.K., Konwar, M., Chakravarty, K., Deshpande, S.M., 2017. Raindrop size distribution of different cloud types over the Western Ghats using simultaneous micro-rain radar and disdrometer observations. Atmos. Res. 186, 72–82. https://doi.org/10.1016/j.atmosres.2016.11.009

Dhar, O. N., Kulkarni, A. K. and Ghose, G. C., 1978, "Rainfall distribution over Indian sub-divisions during the wettest and the driest monsoons of the period 1901-1960", Hydrologiques, Sci. Bul., 23, 2, 213-221.

Distromet, 2002. Disdrometer RD-80 Instruction Manual. Distromet Ltd., Switzerland.

Fletcher, J.K., Parker, D.J., Turner, A.G., Menon, A., Martin, G.M., Birch, C.E., Mitra, A.K., Mrudula, G., Hunt, K.M., Taylor, C.M., Houze, R.A., Brodzik, S.R. and Bhat, G.S. (2020) The dynamic and thermodynamic structure of the monsoon over southern India: new observations from the INCOMPASS IOP. Quarterly Journal of the Royal Meteorological Society, 146, 2867–2890.

Flynn, W.J., Nesbitt, S.W., Anders, A.M., Garg, P., 2017. Mesoscale precipitation characteristics near the Western Ghats during the Indian summer monsoon as simulated by a high-resolution regional model. Q. J. R. Meteorol. Soc. 143, 3070–3084. https://doi.org/10.1002/qj.3163.

Grossman RL and Durran DR (1984) Interaction of low-level flow with the Western Ghat mountains and offshore convection in the summer monsoon. Mon Wea Rev 112: 652–672.

Gunn, R., Kinzer, G.D., 1949. The terminal velocity of the fall of droplets in stagnant air. J. Meteorol. 6, 243–248.

Hersbach, H., Bell, B., Berrisford, P., et al., 2020. The ERA5 global reanalysis. Q.J.R. Meteorol. Soc. 146, 1999–2049. https://doi.org/10.1002/qj.3803.

HeymsBeld G M, Tian L, HeymsBeld A J, Li L and Guimond S (2010) Characteristics of deep tropical and subtropical convection from nadir viewing high altitude airborne Doppler radar; J. Atmos. Sci. 67 285–308.

Houze, R.A., Jr. (1997) Stratiform precipitation in regions of convection: A meteorological paradox? Bull. Amer. Meteor. Soc., 78, 2179–2196.

Houze, R.A., Jr., Wilton, D.C. and Smull, B.F. (2007), Monsoon convection in the Himalayan region as seen by the TRMM Precipitation Radar. Q.J.R. Meteorol. Soc., 133: 1389-1411. https://doi.org/10.1002/qj.106.

Iguchi, T., T. Kozu, R. Meneghini, et al., 2000: Rain-profiling algorithm for the TRMM precipitation radar. J. Appl. Meteor., 39, 2038–2052, doi: https://doi.org/10.1175/1520-0450(2001)040<2038:RPAFTT>2.0.CO;2.

Johnson RH, Ciesielski PE, Hart KA (1996) Tropical inversions near the 0°C level. J Atmos Sci 53:1838–1855

Joss, J., Waldvogel, A., 1967. A spectrograph for raindrops with automatic interpretation. Pure Appl. Geophys. 68, 240–246.

Konwar, M., Das, S.K., Deshpande, S.M., Chakravarty, K., Goswami, B.N., 2014. Microphysics of clouds and rain over the Western Ghats. J. Geophys. Res. Atmos. 119, 1–20. https://doi.org/10.1002/2014JD021606.

Kozu, T., T. Kawanishi, H. Kuroiwa, M. Kojima, K. Oikawa, H. Kumagai, K. Okamoto, M. Okumura, H. Nakatsuka and K. Nishikawa, 2001. Development of precipitation radar onboard the tropical rainfall measuring mission satellite. IEEE Trans. Geosci. Remote Sens., 39, pp.102-116.

Krishnamurthy, V., & Shukla, J. (2000). Intraseasonal and interannual variability of rainfall over India. Journal of Climate, 13(24), 4366–4377. https://doi.org/10.1175/1520-0442(2000)013<0001:IAIVOR>2.0.CO;2.

Kumar, S., Bhat, G.S., 2017. Vertical structure of orographic precipitating clouds observed over South Asia during the summer monsoon season. J. Earth Syst. Sci. 126, 114. https://doi.org/10.1007/s12040-017-0897-9.

Kummerow C, and Coauthors (2000) The Status of the Tropical Rainfall Measuring Mission (TRMM) after Two Years in Orbit. J. Appl. Meteor. Climatol., 39, 1965–1982, https://doi.org/10.1175/1520-0450(2001)040<1965:TSOTTR>2.0.CO;2.

Kummerow C, Barnes W, Kozu T, Shiue J, Simpson J (1998) The Tropical Rainfall Measuring Mission (TRMM) sensor package. J Atmos Ocean Technol 15:809–817.

Maheskumar RS, Narkhedkar SG, Morwal SB, Padmakumari B, Kothawale DR, Joshi RR, Deshpande CG, Bhalwankar RV and Kulkarni JR (2014) Mechanism of high rainfall over the Indian west coast region during the monsoon season. Clim Dyn 43(5–6) 1513–1529.

Marshall JS, Langille RC and Palmer WM (1947) Measurement of rainfall by radar. *J Atmos Sci* 4:186–192. https://doi.org/10.1175/1520-0469(1947)004<0186:MORBR>2.0.CO;2.

Narayana Rao, T., Radhakrishna, B., Nakamura, K., Prabhakara Rao, N., 2009. Differences in raindrop size distribution from southwest monsoon to northeast monsoon at Gadanki. Q. J. R. Meteorol. Soc. 135, 1630–1637.

Parthasarathy, B., Mooley, D. A., 1978: Some features of a long homogeneous series of Indian summer monsoon rainfall.Mon. Wea. Rev. 106, 771–781.

Radhakrishna, B., Rao, T. N., Rao, D. N., Rao, N. P., Nakamura, K., & Sharma, A. K. (2009). Spatial and seasonal variability of raindrop size distributions in southeast India. Journal of Geophysical Research, 114, D04203. https://doi.org/10.1029/2008JD011226.

Rakshit, G., Mohapatra, M., Krishnan, K.S., Maitra, A., 2024. Investigating Monsoon raindrop sizes in relation to associated atmospheric parameters over the Indian Region. Atmos. Res. 304, 107397.

Rao, Y.P., 1976. Southwest Monsoon. Met. Monograph, India Meteorological Department, 367.
Romatschke, U., Houze, R.A. Jr., 2011. Characteristics of precipitating convective systems in the south Asian monsoon. J. Hydrom. 12, 3–25.

Rosenfeld D and Ulbrich C W 2003 Cloud microphysical properties, processes, and rainfall estimation opportunities; In: Radar and Atmospheric Science: A Collection of Essays in Honor of David Atlas, Meteorological Monographs No. 52, the American Meteorological Society, Boston, pp. 237–258.

Saikranthi, K., T.Narayana Rao, B.Radhakrishna, and S. V. B.Rao (2014), Morphology of the vertical structure of precipitation over India and adjoining oceans based on long-term measurements of TRMM PR, J. Geophys. Res. Atmos., 119, 8433–8449, doi:10.1002/2014JD021774.

Salles C and Creutin JD (2003) Instrument uncertainties in Z–R relationships and raindrop fall velocities. J. Appl. Meteor., 42, 279–290.

Schumacher, C., and R. A. Houze (2003) Stratiform Rain in the Tropics as Seen by the TRMM Precipitation Radar. J. Climate, 16, 1739–1756, https://doi.org/10.1175/1520-0442(2003)016<1739:SRITTA>2.0.CO;2.

Sheppard BE and Joe PI (1994) Comparison of raindrop size distribution measurements by a Joss–Waldvogel disdrometer, a PMS 2DG spectrometer, and a POSS Doppler radar. J. Atmos. Oceanic Technol., 11, 874–887.

Shrestha D, Deshar R and Nakamura K (2015) Characteristics of summer precipitation around the Western Ghats and the Myanmar West Coast. International Journal of Atmospheric Sciences,2015, 206016,https://doi.org/10.1155/2015/206016.

Sijikumar, S., and K. Rajeev, 2012: Role of the Arabian Sea warm pool on the precipitation characteristics during the monsoon onset period. J. Climate, 25,1890–1899, https://doi.org/10.1175/ JCLI-D-11-00286.1.

Sreekesh, S., 2016,“Rainfall variation in Lakshadweep Islands”,Indian Journal of Geo-Marine Sciences,45, 11, 1603-1609.

Sridhar, L.; Pai, D.S. Analysis of Long-Term Trends of Rainfall and Extreme Rainfall Events over Andaman & Nicobar and Lakshadweep Islands of India. MAUSAM 2024, 75, 479–500.

Tokay A, Wolff DB , Wolff KR and Bashor P (2003) Rain gauge and disdrometer measurements during the Keys Area Microphysics Project (KAMP). J Atmos Oceanic Technol, 20, 1460–1477.

Tokay, A., Kruger, A., Krajewski, W., 2001. Comparison of drop size distribution measurements by impact and optical disdrometers. J. Appl. Meteorol. 40, 2083–2097. https://doi.org/10.1175/1520-0450(2001)040<2083:CODSDM>2.0.CO;2.

Tokay, A., Short, D.A., 1996. Evidence from tropical raindrop spectra of the origin of rain from stratiform versus convective clouds. J. Appl. Meteorol. 35, 355–371. https://doi.org/10.1175/1520-0450(1996)035<0355:EFTRSO>2.0.CO;2

Utsav B, Deshpande SM, Das SK, Pandithurai G (2017) Statistical Characteristics of Convective Clouds over the Western Ghats Derived from Weather Radar Observations. J Geophys Res Atmos 122:10,050-10,076. https://doi.org/10.1002/2016JD026183.

Xie S-P, HM Xu, NH Saji, YQ Wang and WT Liu (2006) Role of narrow mountains in large-scale organization of Asian monsoon convection. J. Climate, 19, 3420–3429, doi:10.1175/ JCLI3777.1

Yuter SE and Houze RA (1995) Three-dimensional kinematic and microphysical evolution of Florida cumulonimbus. Part II: frequency distributions of vertical velocity, reflectivity, and differential reflectivity. Mon Weather Rev 123: 1941–1963. https://doi.org/10.1175/1520-0493(1995)123<1941:TDKAME>2.0.CO;2.

Zhang G and Smith RB (2018) Numerical study of physical processes controlling summer precipitation over the Western Ghats region. Journal of Climate, 31, 3099–3115.

Figures

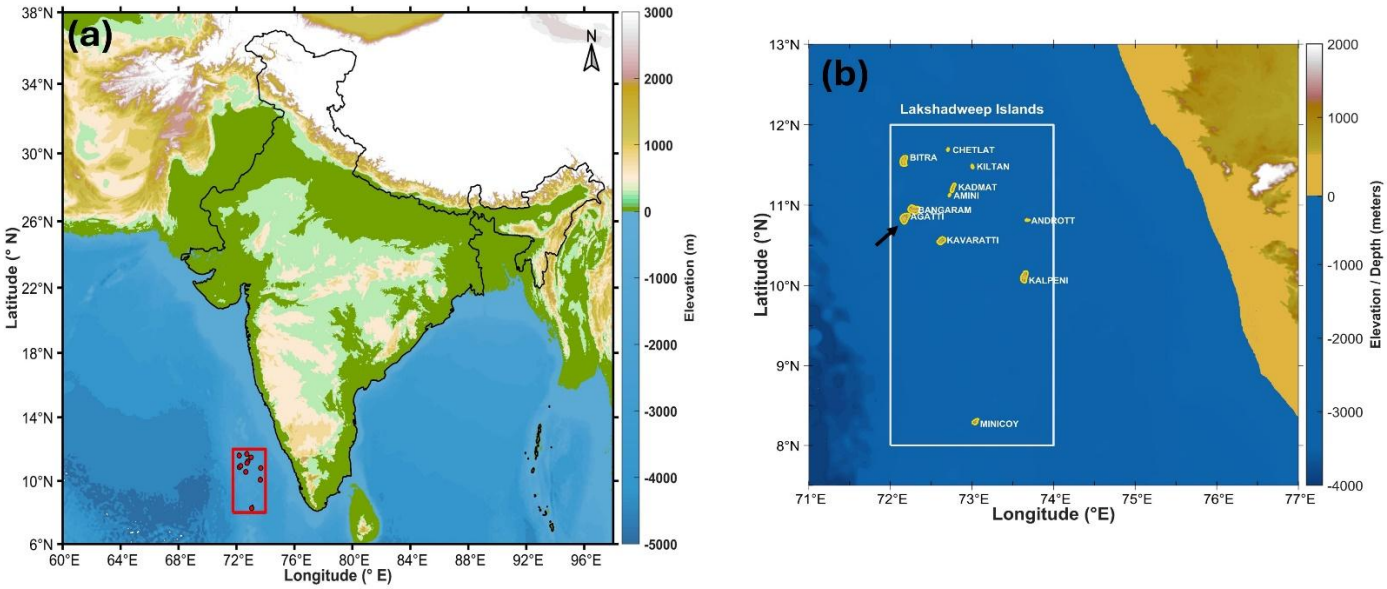
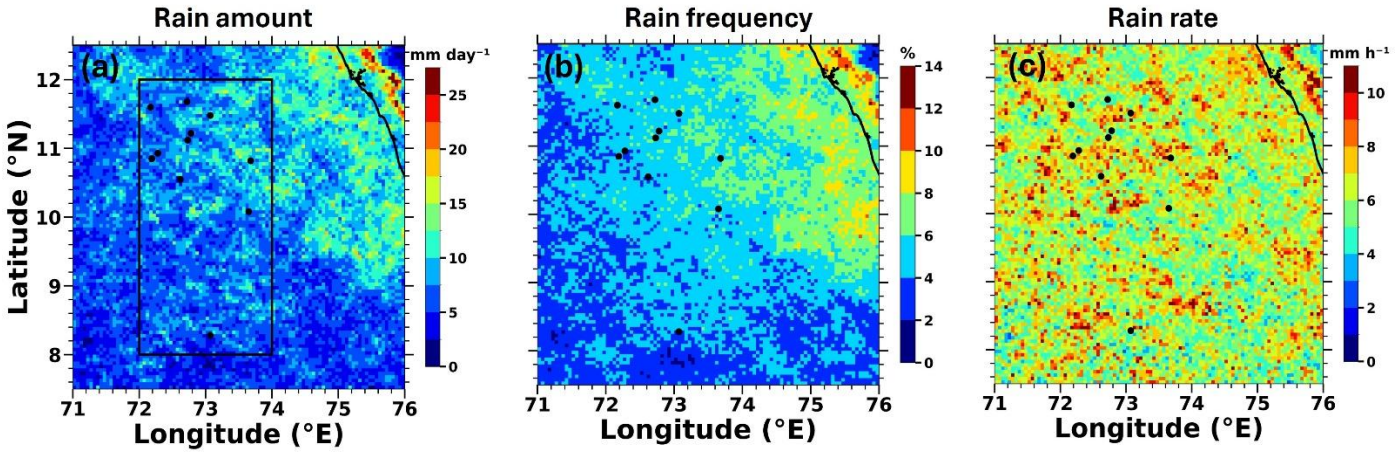


Fig. 1. (a) Topography map of Indian subcontinent with Lakshadweep region highlighted by a red rectangular box. (b) Lakshadweep region enlarged to show the individual islands. The Island marked with arrow is Agatti where disdrometer is installed.



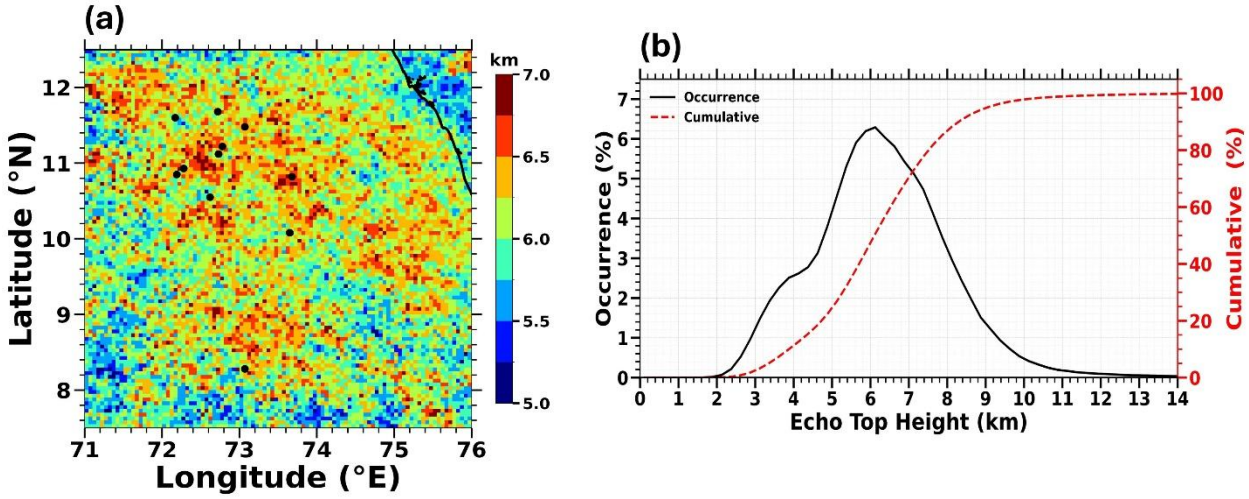
716

717 **Fig. 2.** Spatial distributions of (a) Rain amount (mm/day), (b) Rain frequency (%), and (c) Rain
718 rate (mm/h). Rectangular box (72-74°E, 8-12°N) represents Lakshadweep region considered in
719 this study.

720

721

722



723

724 **Fig. 3.** Spatial distribution of (a) echo top height (km, AMSL). (b) Occurrence frequency of echo
725 top heights along with cumulative occurrence.

726

727

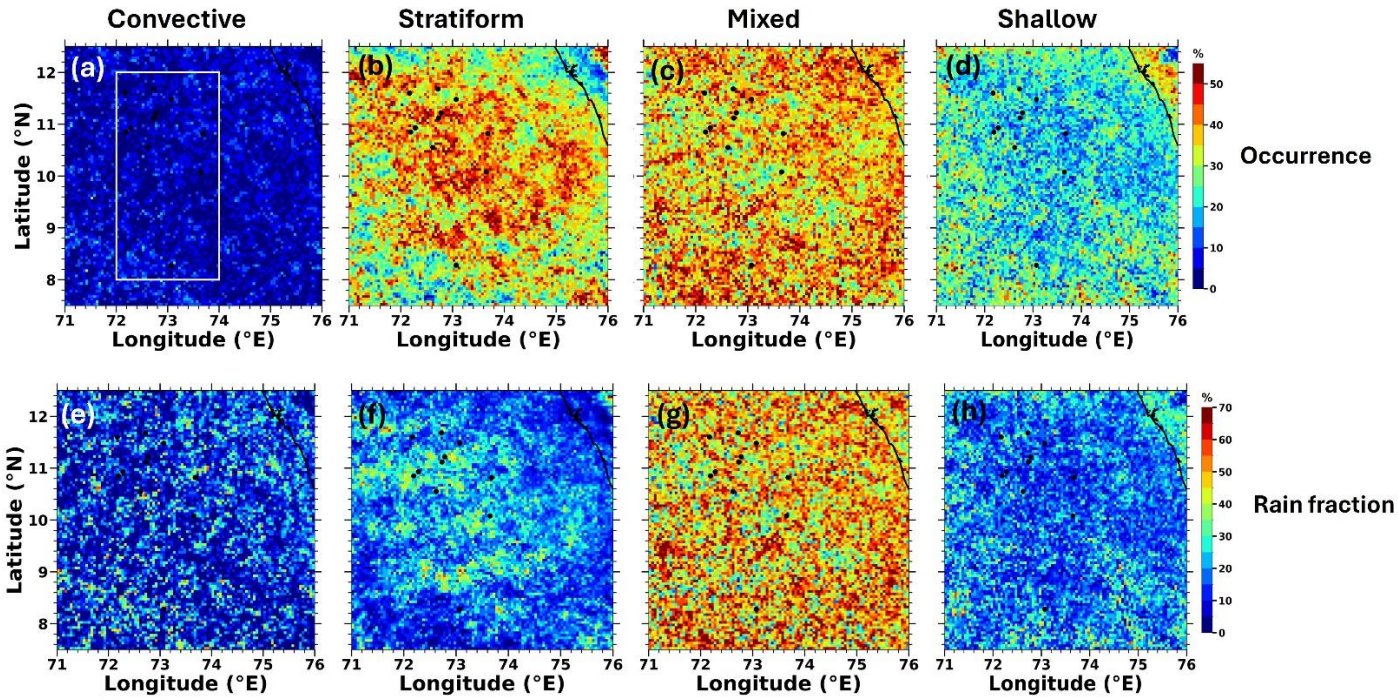


Fig. 4. Spatial distribution of percentage occurrence (a-d) and rain fractions of (e-h) of convective, stratiform, mixed and shallow clouds.

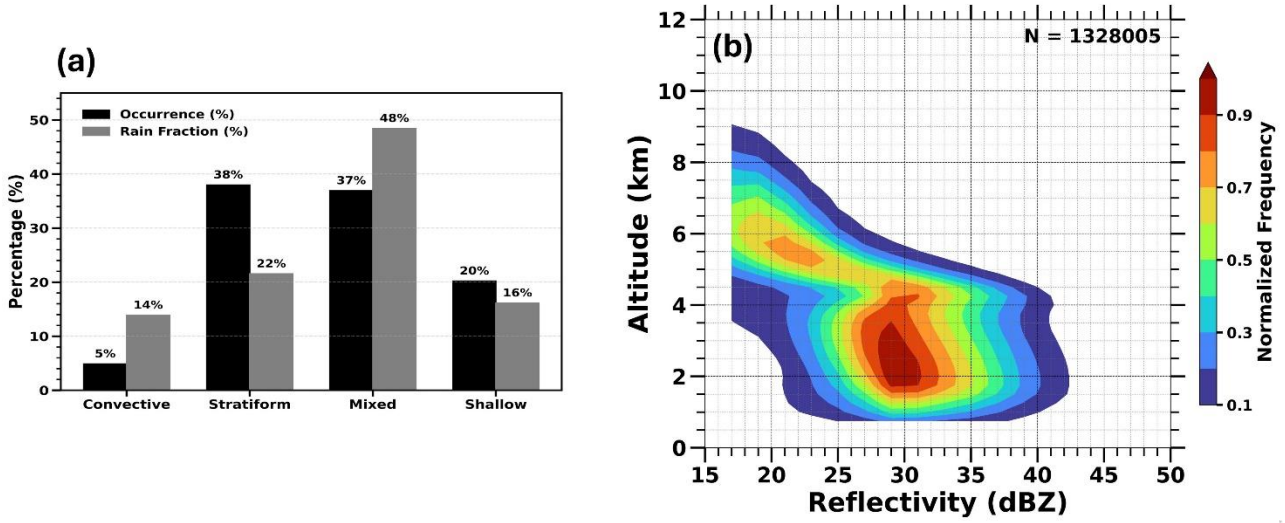


Fig. 5. (a) Cumulative percentage occurrence and rain fractions of different cloud types over LR. (b) Contoured frequency by altitude diagram (CFAD) of Z. The number of Z profiles used to construct CFAD is indicated.

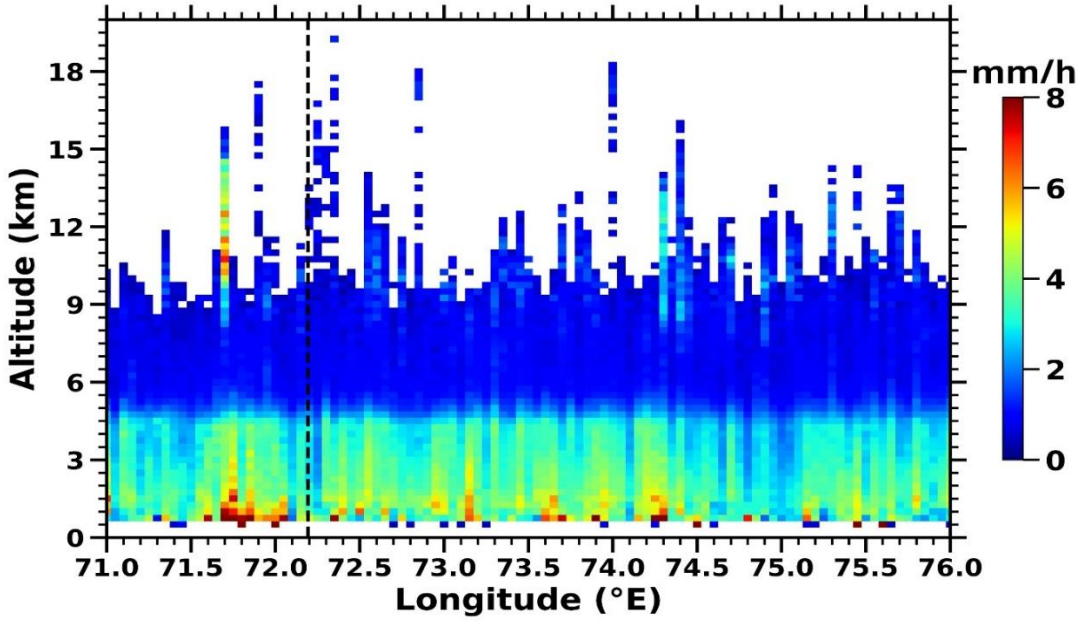


Fig. 6. Vertical cross-section of rain profiles across the latitude of Agatti (shown by dashed vertical line) at 10.8°N.

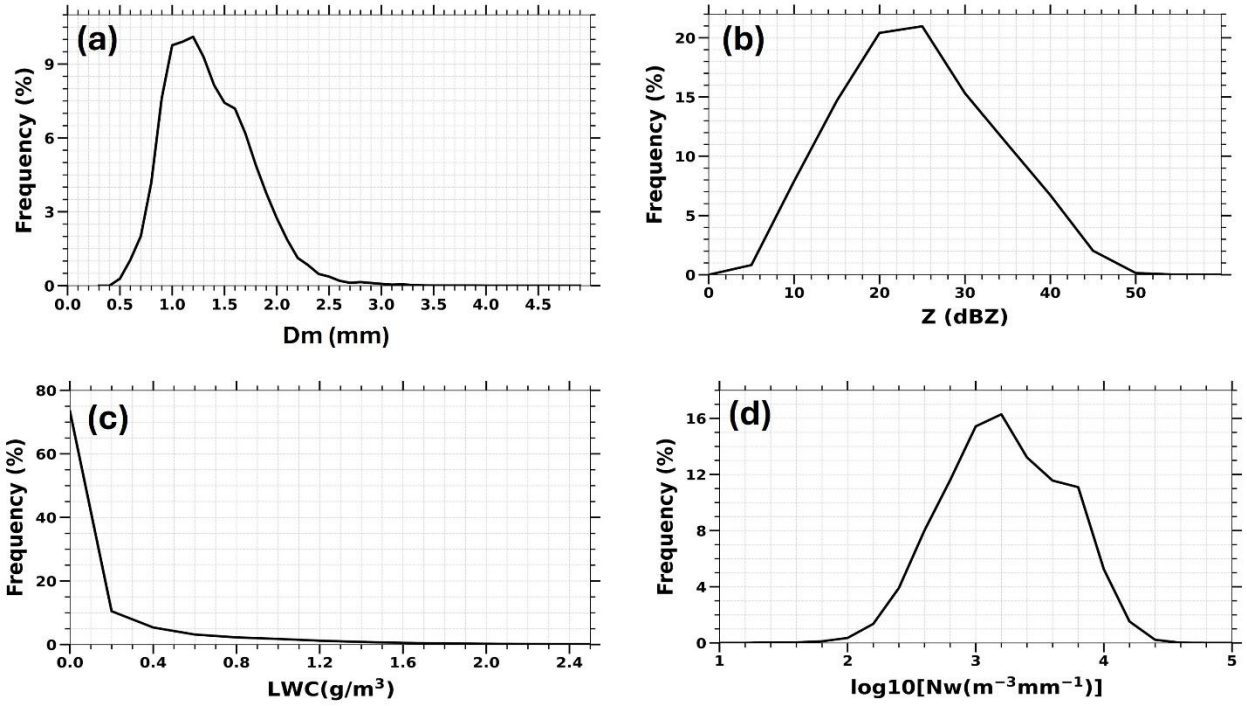


Fig. 7. Frequency distributions of (a) Dm (mm), (b) Z (dBZ), (c) LWC (g/m^3), and (d) log10[Nw(m^{-3} mm^{-1}).

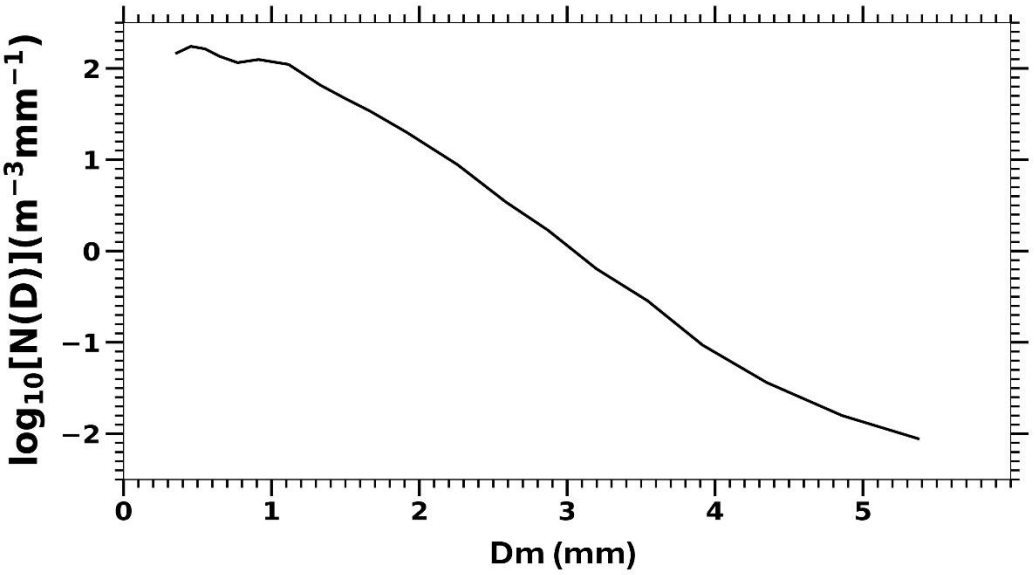


Fig. 8. Mean rain drop size distribution at Agatti.

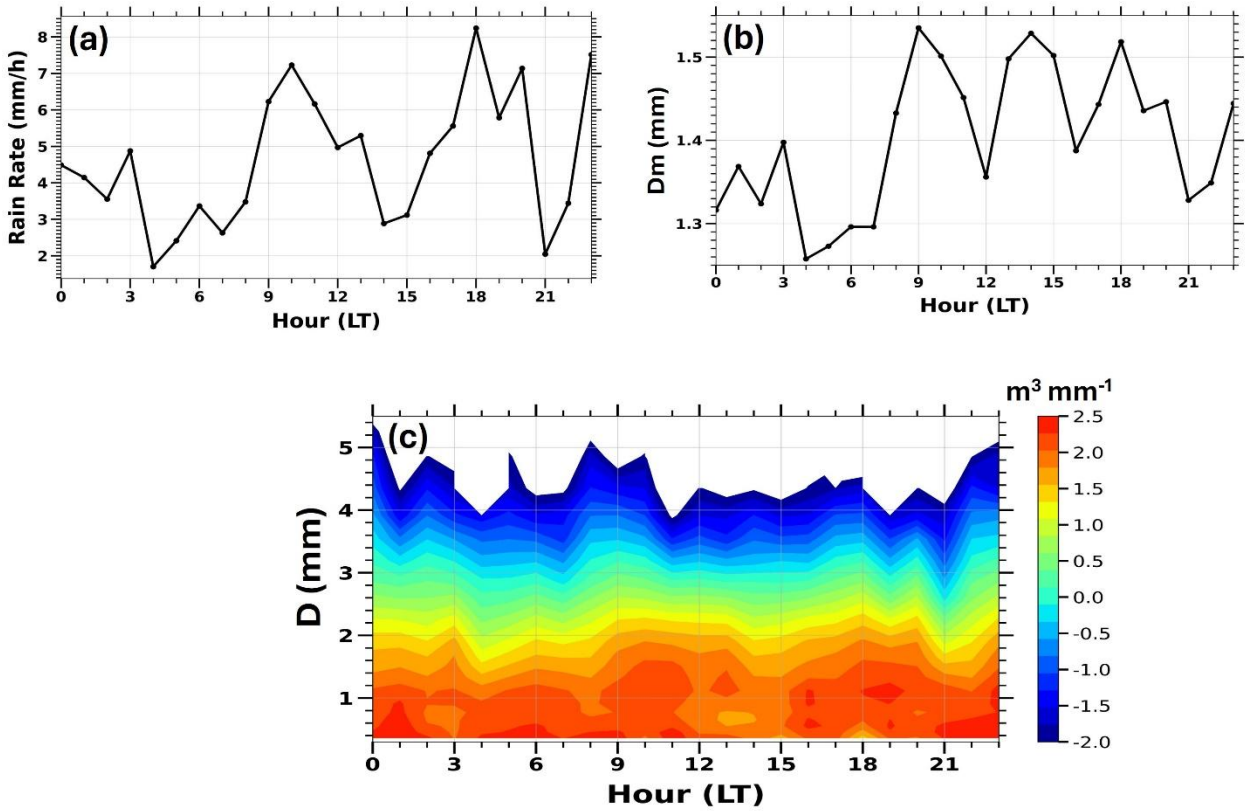


Fig. 9. Diurnal variation of (a) rain rate (mm/h), (b) Dm (mm) and (c) DSD.

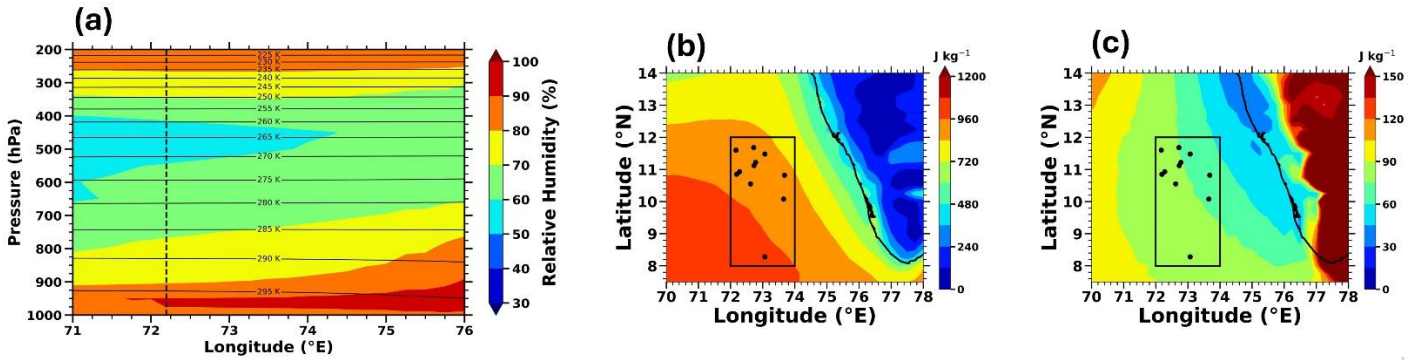


Fig. 10. (a) Pressure-longitude cross section of relative humidity (shadings, %) overlaid with temperature (contours, K) along Agatti at 10.8°N. The location of Agatti is indicated by the dashed vertical line. Spatial distribution of (b) CAPE (J/kg), and (c) CIN (J/kg). The rectangular box indicates the Lakshadweep region.

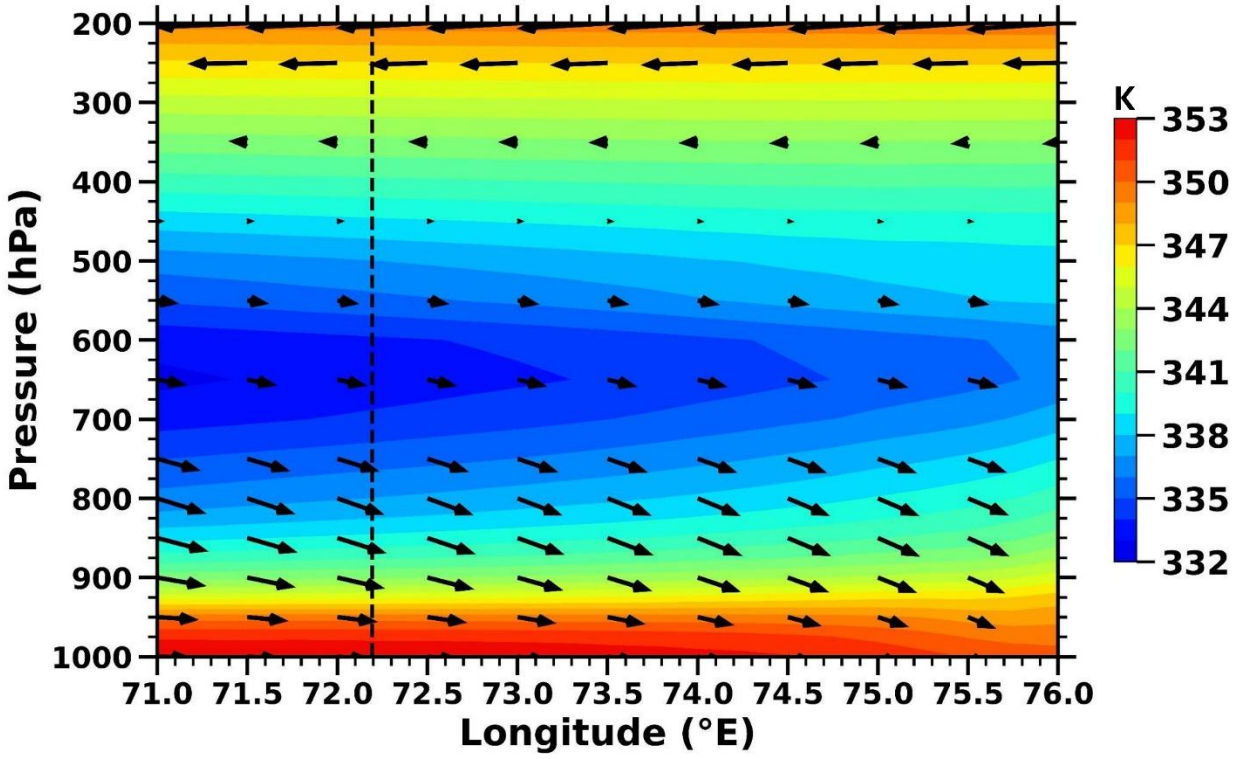


Fig. 11. Pressure–longitude cross-section of equivalent potential temperature (K, shaded) and horizontal wind vectors (m/s, arrows) along Agatti at 10.8°N.